Effect of preparation conditions on short circuits in sol-gel-derived lead titanate thin films

KUNIO SAEGUSA
Tsukuba Research Laboratory, Sumitomo Chemical Company, Tsukuba, Ibaraki 300-32, Japan

A model is proposed by which pore interconnection during firing is responsible for short circuits in thin films. According to this model, the number of short-circuited electrodes can be decreased significantly by suppressing the pore growth, which is achieved by optimizing the hydrolysis conditions of the coating solution and the rapid thermal annealing of the film. At the same time, it became clear that a sol–gel-derived thin film essentially involves a short-circuit probability. The dielectric properties obtained were $\varepsilon = 188$ and $\tan \delta = 8\%$ when fired at 800 °C, for example.

1. Introduction

Ferroelectric thin films have attracted the attention of many researchers in view of their potential application to dynamic random access memories, non-volatile memories and infrared sensors. The sol–gel method is a well-known technique for preparing various thin films [1–13]. These films, however, often have defects that cause short circuits [9, 10], making some applications difficult. Among many mechanisms that cause short circuits, the most important may be defects in thin films (through-holes). Through-holes may be formed in a thin film either by foreign particles or by pore interconnection during sintering. The present paper focuses on the latter and proposes a model that explains how porosity, film thickness and pore size affect the through-hole-forming possibility. Conduction behaviour of a mixture of conducting particles and an insulating matrix is often described by the percolation theory. The present model is based on a similar idea but modified to describe the shortcircuit behaviour better.

In addition, details of preparation conditions of coating solutions and the characterization of thin films in view of the grain and the pore size will be reported since they have not been published previously. The objective of the present work is to prepare non-short-circuited thin films by optimizing the preparation process with the aid of the short-circuiting model. The dielectric properties of thin films will also be reported to show the film quality.

2. Experimental procedure

2.1. Sample preparation

The coating solutions for the present study were prepared according to well-known methods [1, 2]. First 1 mol of lead(II) acetate trihydrate (purity 99.9%; Wako Pure Chemicals, Osaka, Japan) was dissolved into 8 mol (606 g) of 2-methoxyethanol (GR grade; Wako Pure Chemicals) in a four-necked flask under a N_2 atmosphere and distilled at 150 °C for about 2 h until 650 g of the distillate had been recovered. Another 8 mol of 2-methoxyethanol were added to the residual solution and distilled off again. This distillation was repeated three times and the lead concentration was adjusted to 1 mol kg^{-1} (Pb stock solution). Then 1 mol (284 g) of titanium tetraisopropoxide (Wako Pure Chemicals) was dissolved into 500 g of 2-methoxyethanol in a four-necked flask under a N_2 atmosphere and distilled at 150 °C for about 2 h until 400 g of the distillate had been recovered. Another 500 g of 2-methoxyethanol was added to the residual solution and distilled off again. The titanium concentration was adjusted to 1.5 mol kg^{-1} (Ti stock solution).

Next, 0.45 mol of the Pb stock solution and the equimolar Ti stock solution were mixed in a four-necked flask and distilled at 120 °C for 3 h until no distillate was observed. This solution was cooled to 80 °C and distilled at 133 Pa until no distillate came out. The metal concentration of the solution was adjusted to 1 mol kg^{-1} with respect to lead (PT stock solution). Then 3.862 g of H_2O dissolved in 250 g of 2-methoxyethanol with a catalyst (5.165 g of concentrated HNO_3 in the case of acid catalyst) was added to 250 g of the stirred PT stock solution at 80 °C and a rate of 0.73 ml min^{-1} to produce partial hydrolysis. The water-to-titanium ratio ($[H_2O]/[Ti] = R_w$) was 1.3 in this case. The solution was kept at 80 °C for 4 h to mature. Finally, the concentration of the solution was adjusted to 0.65 M with respect to lead by reduced-pressure distillation at 80 °C.

The solution obtained was spin coated on a $Pt(500\ nm)/Ti(50\ nm)/SiO_2(300\ nm)/Si(1\,1\,0)$ substrate on a clean bench (class 100), dried at 130 °C for 15 min and then baked at 300 °C for 30 min in an

0022–2461

infrared heating furnace. The clean bench, air oven, and infrared heating furnaces were located in a clean-room (class 1000) to avoid foreign particles. This procedure was then repeated several times to obtain the desired thickness, and the sample was fired at 500–900 °C with ramp rates ranging from 10 to 600 °C min^{-1} in the rapid thermal annealing (RTA) infrared heating furnace (model RTA-145, Ulvac, Yokohama, Japan).

This solution was allowed to gel, and the gel was dried at 130 °C for longer than 5 h for the thermogravimetry (TG) – differential thermal analysis (DTA) measurement. The dried gel was baked at 300 °C for 30 min and then calcined at a heating rate of 10 °C min^{-1} to prepare powders for X-ray diffractometry (XRD) and Brunauer–Emmett–Teller (BET) measurements.

2.2. Characterization

The crystallization behaviour of the powder was observed by XRD (model RAD-2c, Rigaku-denki Inc., Tokyo, Japan) and TG–DTA (model 2000, MAC Science, Tokyo, Japan). The glancing-angle XRD technique (glancing angle, 0.5°) (model RU-300, Rigaku-denki Inc.) was applied to thin films with Cu Kα radiation (40 kV and 300 mA) monochromated by a silicon single crystal.

The particle size of powders were obtained by BET specific surface area measurements (Quantasorb, Quantachrom Corporation, Syosset, NY) under the

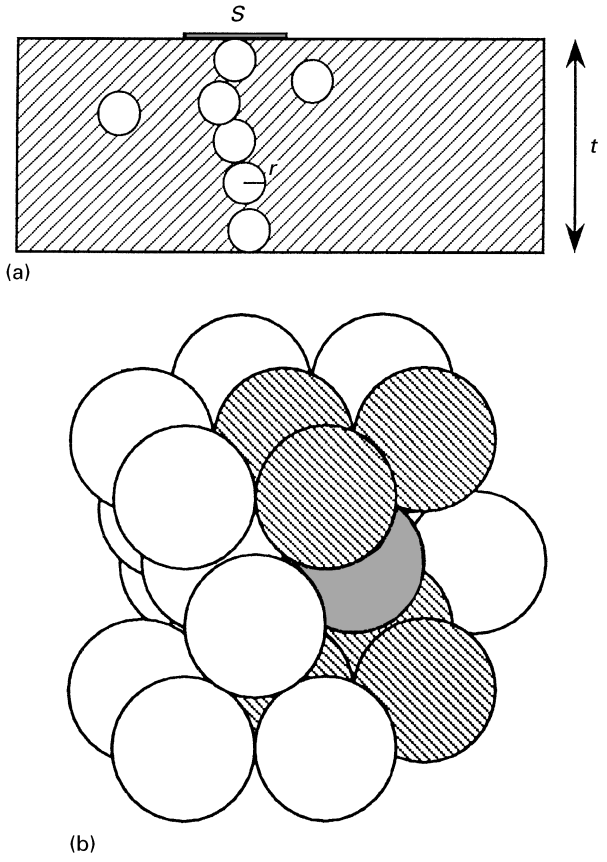

Figure 1 (a) Model of a short-circuit through the association of pores. (b) Pore sites in a close-packed structure. Reference pore site (full circle) and coordinated pore sites (shaded circles) in the adjacent layers.

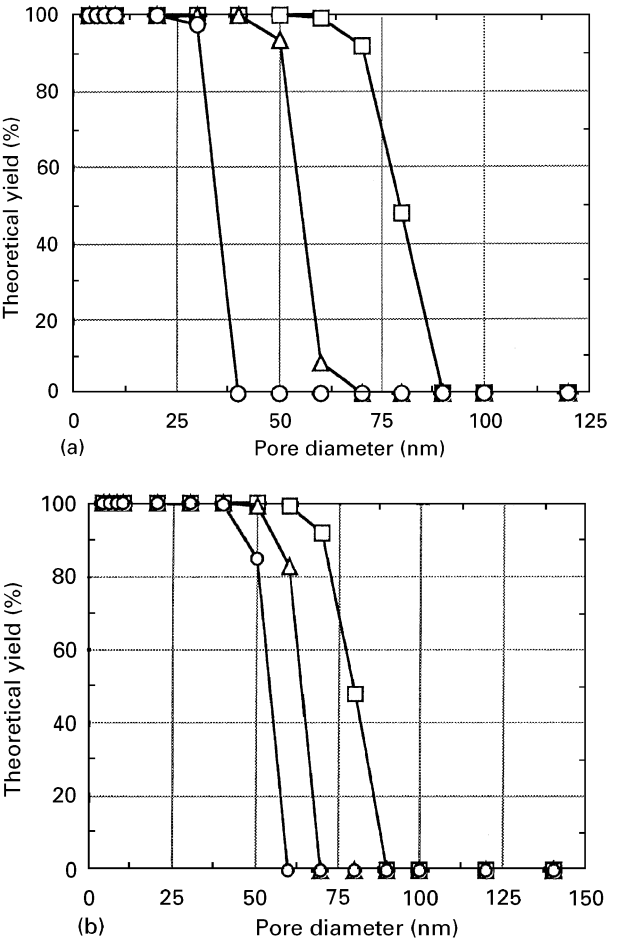

Figure 2 (a) Theoretical yield as a function of pore diameter with film thicknesses of 400 nm (□), 300 nm (△) and 200 nm (○) when $K = 3$, $k = 1.22$ and the porosity equals 0.05. (b) Theoretical yield as a function of pore diameter with porosities of 0.05 (□), 0.075 (△) and 0.1 (○) when $K = 3$, $k = 1.22$ and the film thickness is 400 nm.

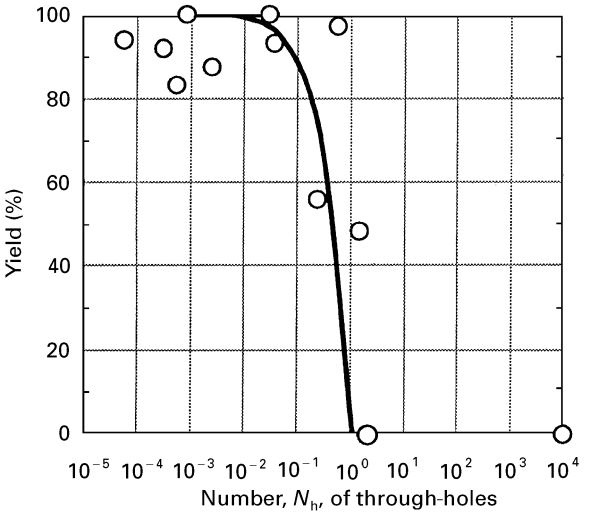

Figure 3 Experimentally obtained yields (○) and theoretical yield curve according to the proposed model as a function of the number, N_h, of through-holes.

assumption that each primary particle was spherical with a $PbTiO_3$ density of 7.96 g cm^{-3}. The grain size and the pore size of the thin films were observed by scanning electron microscopy (SEM) (model JSM-5200, JEOL, Tokyo, Japan) and field-effective

scanning electron microscopy (FESEM) (model S-800, Hitachi, Japan). With the SEM method, the pore size and the porosity were determined using an image analysis (Ultimage, Grafteka, France). Both pore size and porosity have an error of about 20% because of the ambiguity in setting a threshold to convert SEM images into binary images.

Gold was evaporated through mask to form the top electrodes (thickness 100 nm; diameter, 0.3 mm) for the electrical evaluation. Yields (non-short-circuit percentages) were calculated by the number of non-short-circuited electrodes out of the 40 top electrodes in most of the samples. The dielectric constant and tan δ were measured at 0.1 V and 100 kHz using a precision *LCR* meter (model HP-4284A, Hewlett–Packard, San Diego, CA). The remnant polarization and the coercive field were measured using a Sawyer–Tower circuit with a digitizing oscilloscope (model HP-54503A, Hewlett–Packard) and a multifunction synthesizer (model 1920A, NF Electronic Instruments, Yokohama, Japan) at 1 kHz. The film thickness was measured by an etching technique. Part of the $PbTiO_3$ thin film was masked by poly(methyl methacrylate) and then etched with a $HF–H_2O_2$ solution; the etched step height was measured using a surface profilometer.

3. Results and discussion

3.1. Short-circuit model

According to the present model, a short circuit occurs through the interconnection of monosized micropores in thin films during sintering (Fig. 1a). Although there is a pore size distribution in real thin films, it is mathematically difficult to treat the size distribution and the interconnection probability at the same time. Now we assume close-packed pore sites (of radius, r) that can be occupied randomly by the pores of the same size (Fig. 1b). Each layer of the close-packed structure has a thickness, d. Here, K is defined as the coordination number which shows how many pore sites in the adjacent layer are in contact with the reference pore site (see Fig. 1b) ($K = 3$ for the close-packed structure). The probability, p, that the pore contacts with the other pore in the adjacent layer is

$$p = \sum_{i=1}^{K} \frac{{}_{n-K}C_{m-K+i+1}\ {}_{K}C_{K-i+1}}{{}_{n}C_{m}}$$

where n is the number of pore sites and m the number of pores in each layer. When we introduce $P' = m/n$, the nominal porosity, which is based on site occupation, then the probability, p, is P' for $K = 1$, $2P'–P'^2$ for $K = 2$, $3P'–3P'^2–2P'^3$ for $K = 3$, and $4P'–6P'^2 + 4P'^3–P'^4$ for $K = 4$. It can be written as KP' in the approximation when we consider the fact that n, $m \gg 1$, and P' is about 0.1 or less. Here, N_h is defined as the number of through-holes per electrode, t the thickness of the thin film, r the radius of the pores (or pore sites) and S the geometrical area of the electrode. Because t/d layers occur in the thin film, the probability of forming a through-hole by the interconnection of the pores is $(KP')^{t/d-1}$. Since $SP'/4\pi r^2$ pores exist in the area S, N_h can be expressed as

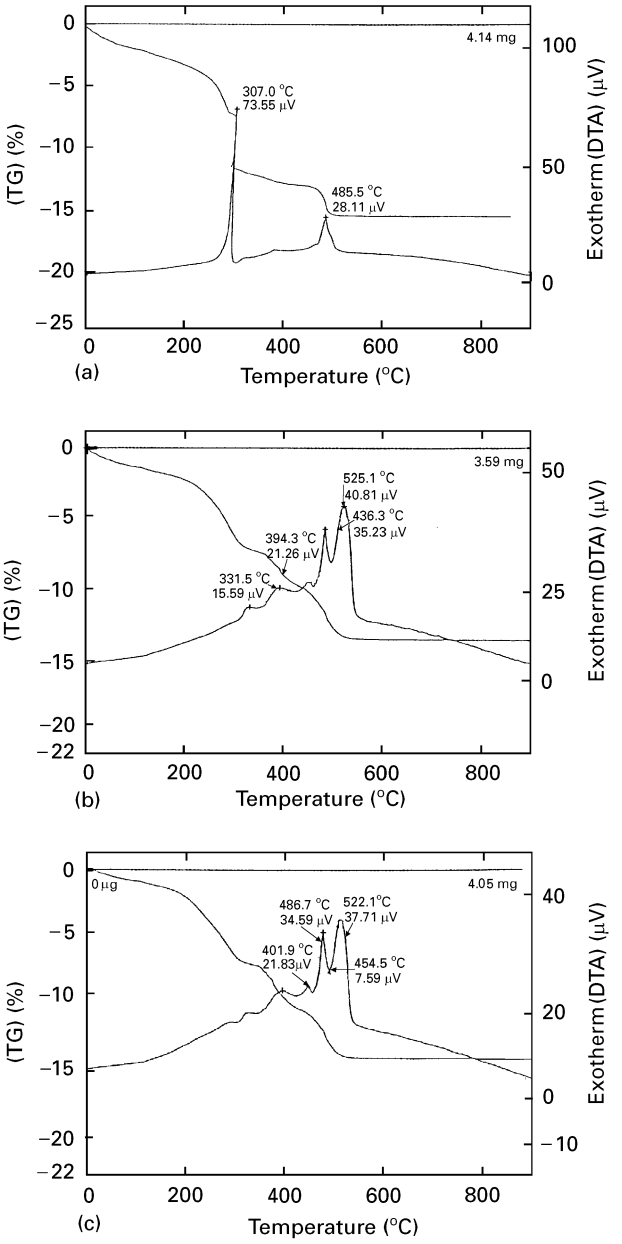

Figure 4 TG–DTA plots of precursor gels hydrolysed under different conditions: (a) HNO_3 catalyst, $R_w = 1.2$; (b) no catalyst, $R_w = 1.2$; (c) NH_3 catalyst, $R_w = 1.2$.

follows when we introduce k to correlate d with r as $d = 2r/k$ ($k = 1.22$ in the case of the close-packed structure):

$$N_h = \frac{K^{(kt/2r)-1}\ S\ r^{-2}\ P'^{(kt/2r)}}{4\pi} \qquad (1)$$

Because only a relatively straight through-hole may contribute to form the conducting path in the electrode deposition, we shall consider only a through-hole that is formed by the pores whose centres are located within a radius, $2r$, from the centre of the reference pore. Then, the equation based on the close-packed structure is

$$N_h = \frac{3^{(kt/4r)-1}\ S\ r^{-2}\ P'^{(kt/2r)}}{4\pi} \qquad (2)$$

Here, P' can be related to P, the real porosity, as $P' = s\ P$, where s is 0.74 in the case of the close-packed

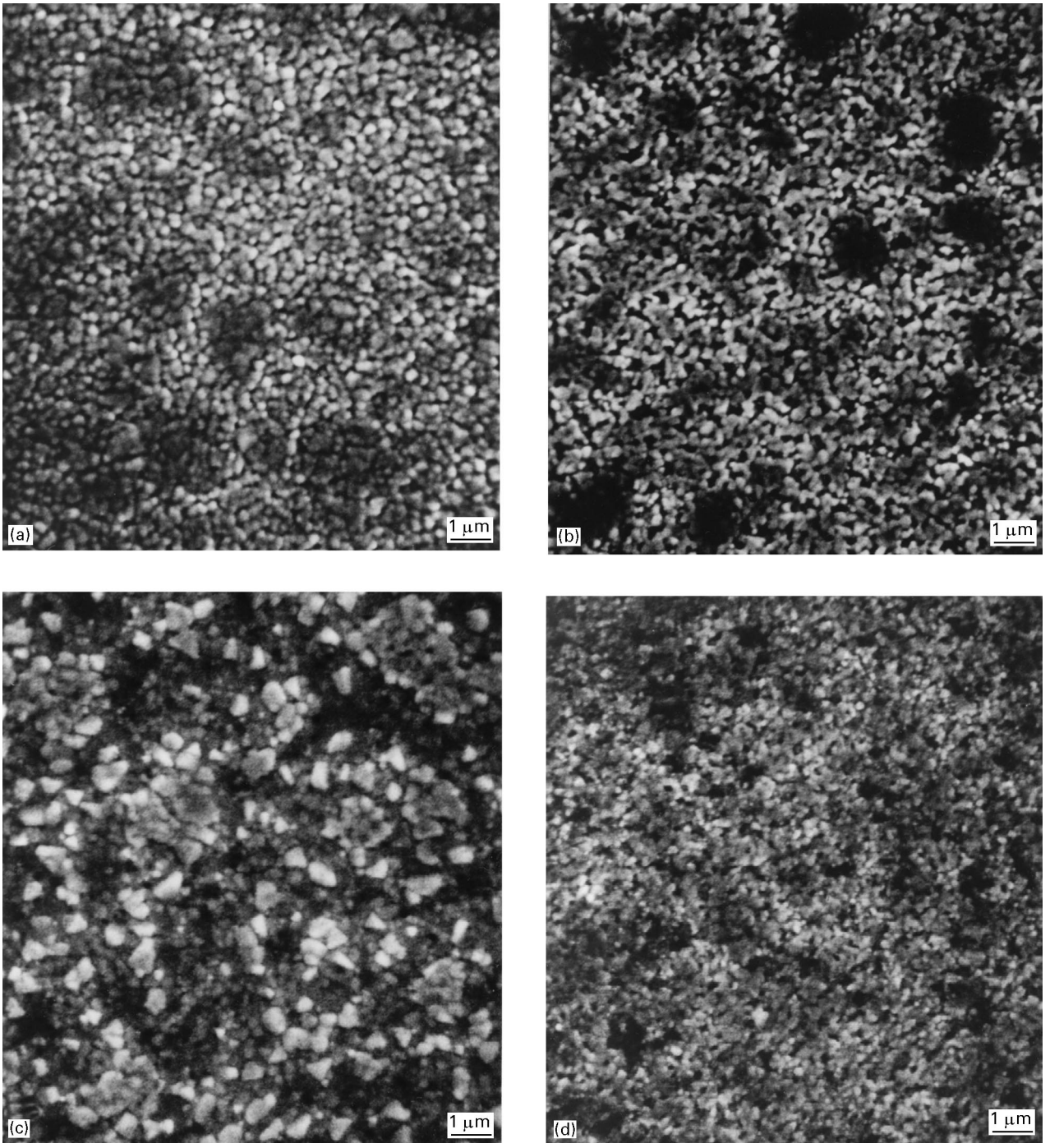

Figure 5 FESEM images of $PbTiO_3$ thin films fired at 650 °C obtained under different hydrolysis conditions: (a) HNO_3 catalyst, $R_w = 1.2$; (b) HNO_3 catalyst, $R_w = 1.3$; (c) NH_3 catalyst, $R_w = 1.2$; (d) NH_3 catalyst, $R_w = 1.5$.

structure since spheres occupy 74 vol % of the whole apparent volume when they are close packed. The number N_h, of through-holes, is strongly dependent on t, P and r as shown in Fig. 2a and b but is not very dependent on k. When short circuits need to be avoided, the pore size must be kept as small as possible, and the film thickness as high as possible. When N_h is larger than one, the theoretical yield is 0% (100% short circuit). Yet the larger N_h may be regarded as reflecting a higher possibility of short circuits in spite of the same theoretical yield of 0%.

According to the model, the number of short circuits can be decreased by attaining low porosity and small pore size. Two approaches have been used to solve the problem. One is to control the precursor gel structure since it is known to affect the structure of a sintered body [1, 2, 11]. The precursor gel structure could be controlled by regulating the hydrolysis conditions (pH and water-to-alkoxide ratio, for example). Another method is the RTA technique, which is considered to be more effective than conventional firing for obtaining a denser structure with a smaller grain size [14, 15].

3.2. Evaluation of proposed model

The measured yields and the theoretical yield curve as a function of N_h are shown in Fig. 3. We may conclude that the proposed model describes the short-circuiting behaviour semiquantitatively well. The pore size, $2r$, the porosity, P, and the thickness, t, of the film were measured and the close-packed structure of pore

sites was assumed for K (= 3) and k (= 1.22) in obtaining the number, N_h, of through-holes by Equation 2. The theoretical and the measured yields as well as other values are summarized in Table I. There are some relatively low measured yields in spite of their low N_h values (equal to high theoretical yields) in Table 1 and Fig. 3. This may be due to the defects introduced by other causes such as foreign particles in the film-forming process. The important fact is that every sample with a theoretical yield of 0% had a measured yield of 0%. This model also seems to describe semiquantitatively the short-circuit behaviour of thin films as a function of the firing temperature, as will be shown later in Figs 6, 7a and 7b.

3.3. Effect of hydrolysis condition

The TG–DTA plots of the precursor gels prepared under different conditions, (i.e., at the same R_w (= 1.2), but with HNO_3 catalyst, no catalyst or NH_3 catalyst), are shown in Fig. 4a, b and c, respectively. The pyrolysis is completed at a lower temperature in the acid-catalysed gel. The base-catalysed gel behaved similarly to the gel without catalysts. Fig. 5 shows the FESEM images of $PbTiO_3$ thin films fired at 650 °C that were hydrolysed with different catalysts. When $R_w > 1.5$ in the ammonia-catalysed solution, the solution was unstable and easily gelled before use. In the case of the HNO_3 catalyst, the precursor solution gelled when $R_w = 1.5$, and the highest possible R_w was 1.3. The grain size was similar but the porosity was slightly higher in the case of $R_w = 1.2$ when compared with $R_w = 1.3$ with acid catalysts.

The highest R_w with the ammonia catalyst resulted in the smallest grain size (equal to the pore size) in fired thin films. Fig. 6a shows the yield as a function of the firing temperature and the hydrolysis conditions. The yield was higher when the pore size was smaller. The film that had the smallest pores ($R_w = 1.5$) had the highest yield.

This may be explained by the difference in the precursor gel structure. In general, the higher the R_w is, the higher the molecular weight of alkoxide polymer becomes (in other words, the larger the sol particle becomes). When the sol particles are very small, they tend to develop greater coalescence during the drying process, which result in a coarse sintered structure (larger grains) because of the extremely high surface energy of the fine sol-particle [11]. This phenomenon is rooted in the fractal nature of gels. Therefore, relatively large sol particles in the precursor, which correspond to a high R_w, remain less coalescent during drying and early-stage sintering and are favourable for smaller grains after sintering. Although the XRD patterns of these samples are similar to each other, the acid-catalysed gels or the gels of higher R_w seemed to have steeper XRD peaks, showing better crystallization (Fig. 7).

3.4. Rapid thermal annealing

The theoretical yield was calculated by the proposed equation using the experimentally obtained data such

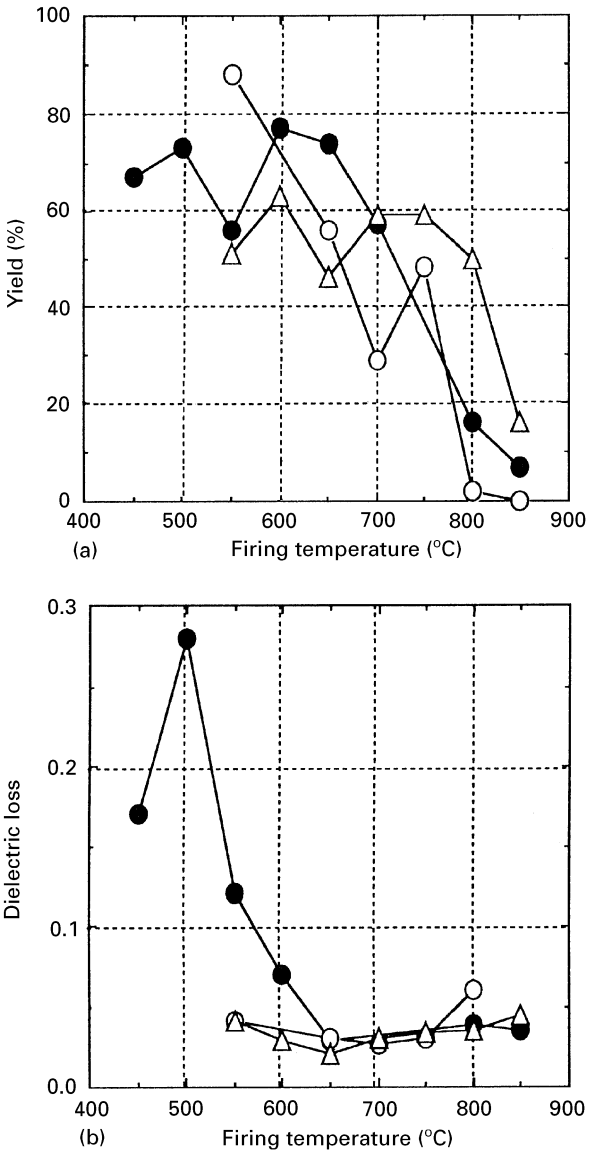

Figure 6 (a) Yield and (b) dielectric loss as functions of firing temperature (heating rate, 10 °C min^{-1}) under different hydrolysis conditions (●), HNO_3 catalyst, $R_w = 1.2$; (○), NH_3 catalyst, $R_w = 1.2$; (△), NH_3 catalyst, $R_w = 1.5$.

as the pore diameter, the film thickness, and the porosity of the thin films fired at a heating rate of 10 °C min^{-1}. The yields experimentally obtained for thin films fired at 10 and 600 °C min^{-1} are shown in Fig. 8. The theoretical yield matches the measured yield fairly well as a function of the firing temperature (through the pore size), showing that the proposed model is applicable. The heating rate of 600 °C min^{-1} increased the yields significantly in both the 100 nm and the 200 nm thin films, as shown in Fig. 8. Fig. 9a and b shows the microstructure of thin films obtained by heating rates of 10 °C min^{-1} and 600 °C min^{-1}, respectively. The film that was fired by the RTA technique had the smaller pore size and the more uniform structure.

However, with respect to large scale production, the attaining of defect-free thin films by a sol–gel process can be very difficult because the short-circuit probability will not reach zero. During densification, the film has to reduce its volume by more than 40% in the sol–gel process. Being constrained by the substrate,

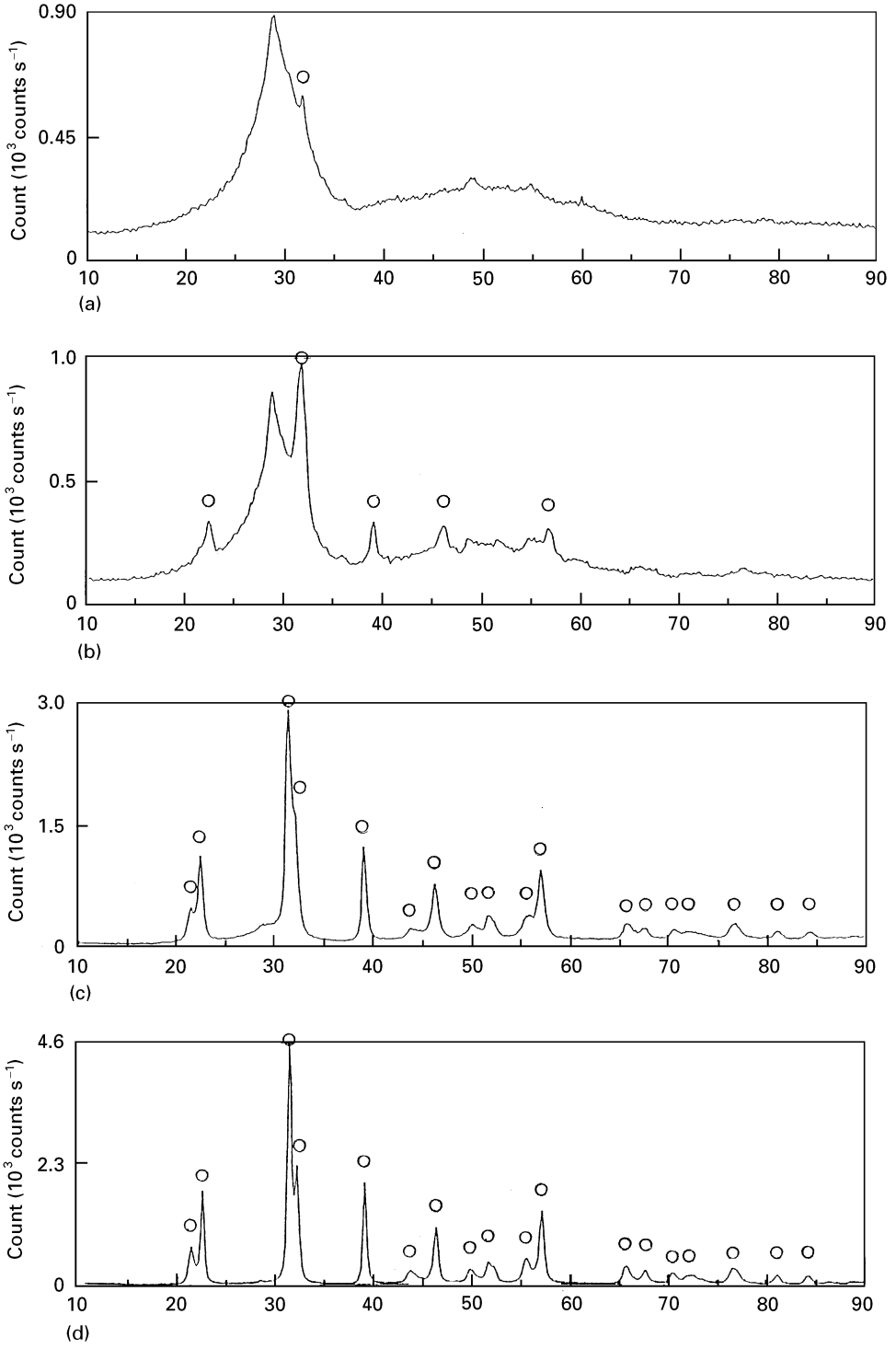

Figure 7 XRD patterns of $PbTiO_3$ Powders calcined at (a) 450 °C, (b) 500 °C, (c) 550 °C and (d) 600 °C.

the film contracts mainly perpendicular to the substrate, but there remains a force in the film to contract parallel to the substrate and the force has to be relaxed to avoid a crack. Pores must play an important role in relaxing the stress between the film and the substrate. In other words, a film will crack without a certain degree of porosity, which means that the short-circuit probability will not reach zero. Although it may be possible to keep the porosity so low that the short-circuit problem can be almost avoided, even the least probability may cause a significant number of defects during large-scale production.

3.5. Particle size, grain size and crystal phase change on firing

The spherical particle size calculated from the surface area of $PbTiO_3$ powder generally agreed well with the grain size of $PbTiO_3$ thin films determined by SEM observation when they were fired at temperatures below 700 °C (Fig. 10). This is probably because each primary particle may have formed a single grain at the firing temperature but has not yet begun to be sintered. The particle size of $PbTiO_3$ was 50 nm at 500 °C and 160 nm at 800 °C in the normal sintering condition.

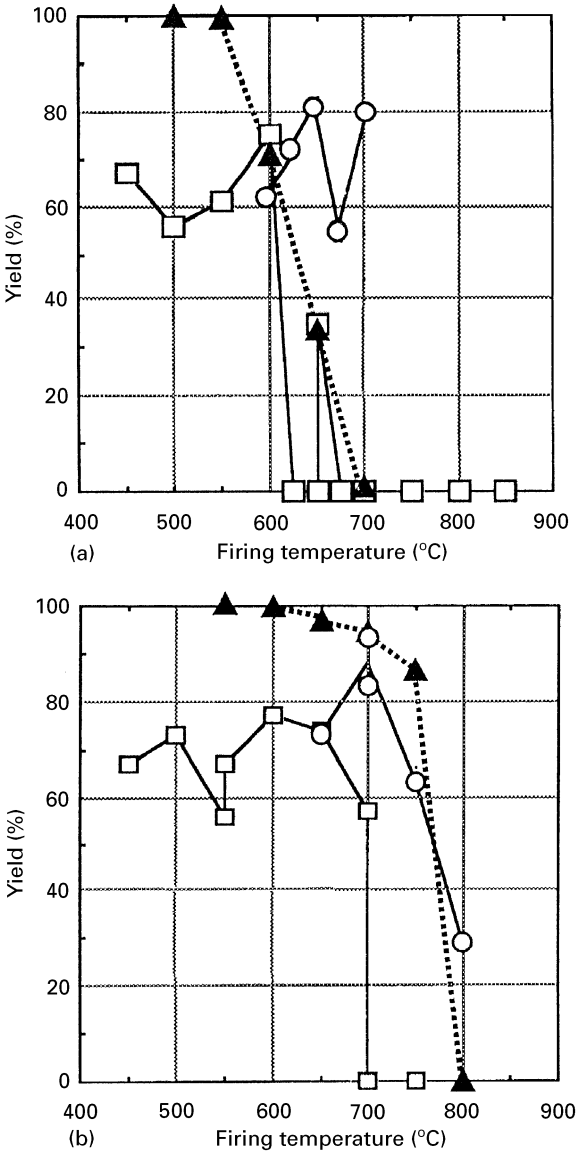

Figure 8 Yields of thin films at heating rates of 10 °C min^{-1} (□) and 600 °C min^{-1} (○), and the theoretical yield based on the 10 °C min^{-1} data (▲) as functions of the firing temperature: (a) film thickness of 100 nm; (b) film thickness of 200 nm.

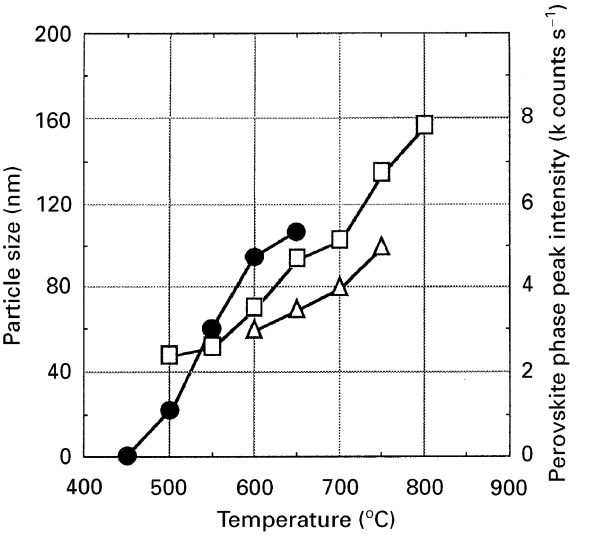

Figure 10 Perovskite phase evolution (●), particle size (□) and grain size (△) of $PbTiO_3$ as functions of the firing temperature.

The perovskite phase evolution (peak intensity of XRD) as a function of temperature is also shown in Fig. 10. Fig. 7 shows XRD patterns of the $PbTiO_3$ powders fired at temperatures in the range 450–600 °C. The effect of the firing temperature apparently was critical. The higher the firing temperature used, the larger the particles and the grain size were and the higher the perovskite phase content became (Figs 7 and 10). The pyrochlore phase was dominant at 450 and 500 °C and then almost disappeared at 550 °C. The perovskite phase was observed first at 450 °C, then it became prominent at 500 °C, and it crystallized well at or above 600 °C. The perovskite peaks became sharper and more intense at a higher firing temperature, as shown in Figs 7 and 11.

Examples of the dielectric properties and the XRD plots of the thin films are shown in Table I and Fig. 11. The film with good quality was obtained in terms of the dielectric properties. For example, $\varepsilon = 190$ and $\tan\delta = 8\%$ when the film was fired at 800 °C.

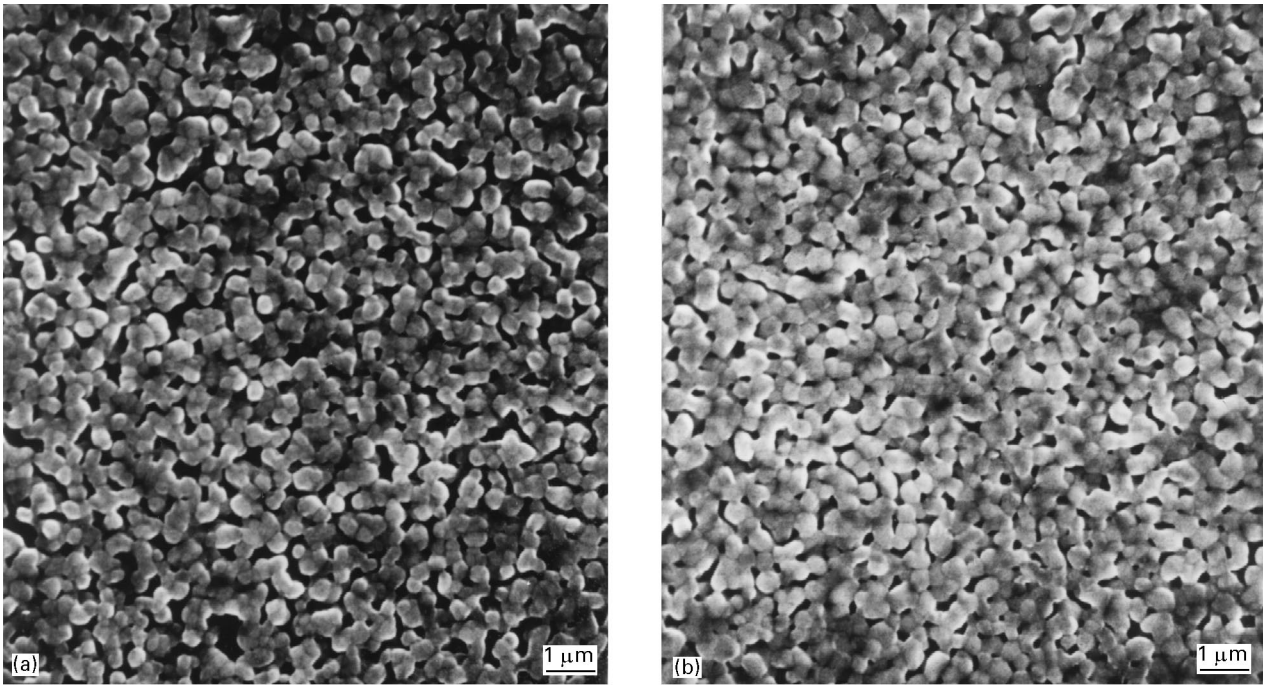

Figure 9 SEM images of $PbTiO_3$ thin films fired at 800 °C at heating rates of (a) 10 °C min^{-1} (yield; 0%) and (b) 600 °C min^{-1} (yield, 96%).

TABLE I Short-circuit behaviour and electrical properties of $PbTiO_3$ thin films

Sample	Film thickness (nm)	Firing temperature (°C)	Heating rate (°C min^{-1})	Porosity (%)	Pore size (nm)	Calculated short N_h	Theoretical yield (%)	Measured yield (%)	Dielectric constant	Dielectric loss
201ZB	155	700	10	14	41	9.6×10^{3}	0	0		
302E	180	650	10	4	33	2.4×10^{-1}	76	56	206	0.03
303D	250	650	10	9	42	1.4×10^{-1}	86	46	235	0.02
801D	330	600	10	11	28	8.4×10^{-4}	100	100	164	0.19
801V	306	600	10	7	32	3.0×10^{-4}	100	92	158	0.141
801T	307	700	10	18	38	5.3×10^{-4}	100	83.3	196	0.049
801U	330	800	10	11	40	2.1	0	0		
801E	420	700	600	4	23	2.1×10^{-4}	100	96	192	0.27
801F	440	700	600	12	53	5.7×10^{-1}	43	97	190	0.19
801G	391	800	600	6	28	1.3×10^{-10}	100	96	188	0.08
801L	403	800	600	12	42	5.7×10^{-5}	100	94	175	0.081
801K	400	900	600	5	65	3×10^{-2}	97	100	288	0.12
801N	400	900	600	10	50	3.7×10^{-2}	96	93	155	0.026

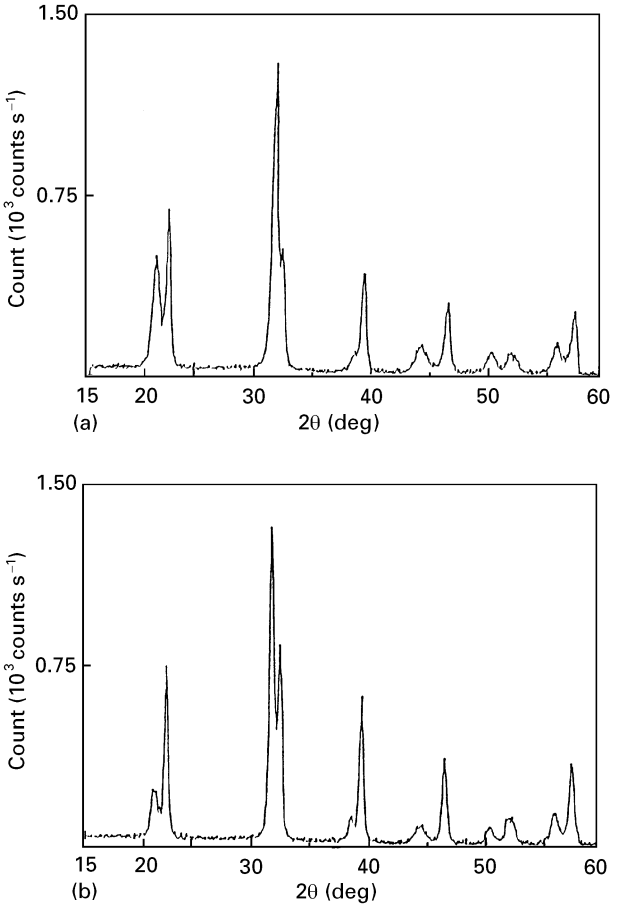

Figure 11 XRD patterns and electrical properties of $PbTiO_3$ thin films fired at (a) 600 °C ($\varepsilon = 149$; $\tan\delta = 0.19$) and (b) 800 °C ($\varepsilon = 163$; $\tan\delta = 0.056$).

4. Conclusions

1. A model consisting of interconnected pores that create a through-hole in a film matrix seems to describe suitably the short-circuit behaviour of thin films.

2. The high $R_w(=1.5)$ obtained with ammonia as a catalyst during partial hydrolysis of the coating solution effectively kept the pore size small and reduced short circuits in the present experiment.

3. The RTA technique (600 °C min^{-1}) was effective for reducing short circuits.

4. The film quality was so good that it showed dielectric properties such as $\varepsilon = 190$ and $\tan\delta = 8\%$ when fired at 800 °C.

5. With respect to large-scale production, it seems difficult to attain defect-free sol–gel-derived thin films because the short-circuit probability will not reach zero.

Acknowledgements

The author would like to acknowledge Mr Suzuki, Mr Honda, Dr Oishi and Mr Shiraga at Sumitomo Chemical company for their contributions.

References

1. K. D. BUDD, S. K. DEY and D. A. PAYNE, *Brit. Ceram. Proc.* **36** (1985) 107.
2. *Idem.*, *Mater. Res. Soc. Symp. Proc.* **72** (1986) 317.
3. Y. HAYASHI and J. BLUM, *J. Mater. Sci.* **22** (1987) 2655.
4. R. W. VEST and J. XU, *IEEE Trans. Ultrason., Ferroelectr. Frequency Control* **35** (1988) 711.
5. C. CHEN and D. F. RYDER Jr, *J. Amer. Ceram. Soc.* **72** (1989) 1495.
6. S. L. SWARTZ, P. J. MELLING and C. S. GRANT, *Mater. Res. Soc. Symp. Proc.* **152** (1989) 227.
7. S. J. MILNE and S. H. PYKE, *J. Amer. Ceram. Soc.* **74** (1991) 1407.
8. N . TOHGE, S. TAKAHASHI and T. MINAMI, *ibid.* **74** (1991) 67.
9. S. S. DANA, K. F. ETZOLD and J. CLABES, *J. Appl. Phys.* **69** (1991) 4398.
10. L. E. SANCHEZ, D. T. DION, S. Y. WU and I. K. NAIK, *Ferroelectrics* **116** (1991) 1.
11. M. D. CARPER and P. P. PHULE, *Appl. Phys. Lett.* **63** (1993) 153.
12. M. MAEDA, H. ISHIDA, K. KO, K. SOE and I. SUZUKI, *Jpn. J. Appl. Phys. Part* 1 **32** (1993) 4136.
13. C. R. CHO, M. S. JANG, S. Y. JEONG and Y. B. KIM, *Cryst. Res. Technol.* **28** (1993) 1085.
14. C. K. BARLINGAY and S. K. DEY, *Ceram. Trans.* **25** (1992) 265.
15. Z. WU, R. PASCUAL, C. V. R. V. KUMAR, D. AMM and M. SAYER, *Mater. Res. Soc. Symp. Proc.* **224** (1991) 305.

Received 8 October 1996
and accepted 1 May 1997